The molecular basis for peptide repertoire selection in the Human Leucocyte Antigen (HLA) C*06:02 molecule

Jesse I. Mobbs[1], Patricia T. Illing[1], Nadine L. Dudek[1], Andrew G Brooks[2,] Daniel G Baker[3], Anthony W. Purcell[4], Jamie Rossjohn[4*] Julian P. Vivian[1]

Author Affiliations

[1] Infection and Immunity Program & Department of Biochemistry and Molecular Biology Biomedicine Discovery Inst, Monash University, Australia;
[2] Department of Microbiology and Immunology, University of Melbourne, Peter Doherty Inst for Infection and Immunity, Australia;
[3] Janssen R&D, Philadelphia, United States;
[4] Australian Research Council Centre of Excellence in Advanced Molecular Imaging, Monash University, Australia
[5] Institute of Infection and Immunity, Cardiff University, Cardiff UK

Keywords: immunology, major histocompatibility complex (MHC), antigen presentation, crystal structure, mass spectrometry (MS), HLA-C*06:02

ABSTRACT

Human Leucocyte antigen (HLA) C*06:02 is identified as the allele associated with the highest risk for the development of the autoimmune skin disease psoriasis. However, the diversity and mode of peptide presentation by the HLA-C*06:02 molecule remains unclear. Here, we describe the endogenous peptide repertoire of approximately 3,000 sequences for HLA-C*06:02 that defines the peptide-binding motif for this HLA allomorph. We found that HLA-C*06:02 predominantly presents nonamer peptides with dominant arginine anchors at the P2 & P7 positions and a preference for small hydrophobic residues at the C-terminus (PΩ). To determine the structural basis of this selectivity, we determined crystal structures of HLA-C*06:02 in complex with two self-peptides (ARTELYRSL and ARFNDLRFV) and an analogue of a melanocyte auto-antigen (ADAMTSL5, VRSRR-abu-LRL) implicated in psoriasis. These structures revealed that HLA-C*06:02 possesses a deep peptide-binding groove comprising two electronegative B- and E-pockets that coincide with the preference for P2 and P7 arginine anchors. The ADAMTSL5 autoantigen possessed a P7-Leu instead of the P7-Arg residue, but nevertheless was accommodated within the HLA-C*06:02 antigen-binding cleft. Collectively, our results provide the structural basis for understanding peptide repertoire selection in HLA-C*06:02.

INTRODUCTION

The Major Histocompatibility Complex (MHC) class I locus (human leukocyte antigen (HLA)-I in humans) encodes highly polymorphic molecules that present antigenic peptides to both the adaptive and the innate arms of the immune system. Expressed on all nucleated cells, HLA-I present peptides derived from the cytosolic turnover of proteins that are surveyed by αβ T-cell receptors on cytotoxic T-cells to monitor for metabolic or pathogenic transformation. Complementing this system, natural killer cells (NK) express inhibitory Killer-cell immunoglobulin-like receptors (KIR) that monitor for HLA-I expression, thereby ensuring that immune surveillance cannot be subverted via down-regulation of HLA-I [1, 2]. The polymorphic sites within HLA-I molecules are generally clustered within the peptide-binding groove facilitating the presentation of diverse peptide repertoires within individuals and across the population [3–6]. The breadth in HLA-I diversity can result in idiosyncratic HLA-associated pathologies like drug hypersensitivities and autoimmune disorders. For example, abacavir hypersensitivity is associated with HLA-B*57:01 [7], Birdshot Retinochoroidopathy with HLA-A*29:02 [8], Ankylosing Spondylitis with HLA-B*27:05 [9], and psoriasis with HLA-C*06:02 [10]. Autoimmune disorders are typically multifactorial; as such the identification of specific autoantigens has been difficult. Nonetheless, progress has been made identifying insulin epitopes in diabetes [11, 12] and in the setting of CD4+T-cell recognition of specific autoantigenic epitopes presented by HLA-II molecules. For example, the presentation of citrullinated self-epitopes by HLA-DRB1*04:01/04 in rheumatoid arthritis [13, 14] and the presentation of deamidated peptides derived from dietary gluten by HLA-DQ8 and HLA-DQ2 in celiac disease [15–17]. However, although the genetic associations are often compelling, the molecular "triggers" and autoantigens for many HLA-I-associated autoimmune disorders have remained elusive.

In comparison to the HLA-A an HLA-B allomorphs, HLA-C is relatively under-represented in terms of available peptide repertoire and structural data. The current data suggests that HLA-C presents a more restricted repertoire of peptides and has a strong preference for nonamers [18–20]. However, as Rasmussen *et al.* [18] have noted these generalizations are based on limited data as HLA-C represents <3% of the peptide repertoire data in the Immune Epitope Database [21]. Similarly, in the Protein Data Bank there are only five peptide-HLA-C structures currently deposited [22]. This disparity is partly attributable to studies on T-cell recognition tending to focus on HLA-A and HLA-B that are expressed on the cell surface at 3–10-fold higher levels than HLA-C [23, 24]. Furthermore, studies into HLA-C have centered on it being primarily a ligand for the lineage III KIR on NK cells [1]. Therefore, whereas there is an emerging appreciation of the

role of HLA-C in T-cell-mediated events in viral immunity and psoriasis (reviewed in Ref. 25), there remains a paucity of peptide repertoire and structural information.

Psoriasis has a complex genetic component with more than 20 regions of risk identified by genome-wide association studies. Of these, psoriasis susceptibility locus 1 (PSORS1) has the highest risk association and maps to the region of *HLA-C* [26]. More than 60% of psoriasis patients carry the *HLA-C*06:02* allele that is linked with early onset of the disease, with *C*06:02* homozygotes having a 5-fold higher risk association than heterozygotes [27, 28]. Although tentative associations have been made to the activating lineage III KIR [1, 29–31], psoriasis is nonetheless considered a predominantly T-cell-mediated disease that manifests as increased proliferation and abnormal differentiation of keratinocytes as well as infiltration of inflammatory immune cells into the skin [26, 32–34]. Furthermore, environmental factors including prior streptococcal infection are linked with disease onset [35]. Accordingly, the search for *HLA-C*06:02* restricted autoantigens has focused on skin-related peptides such as those arising from the antimicrobial LL-37 peptide [36] and the ADAMTSL5 melanocyte protein [37] as well as streptococcal M-protein "molecular mimics" of keratin peptides [38, 39]. To date, the identification and validation of specific antigenic peptides has been hampered by a lack of structural data on the architecture of the HLA-C*06:02 peptide-binding groove and the defining features that drive selection of its peptides repertoire.

Here we have utilized high-resolution mass spectrometry to identify native peptides of HLA-C*06:02 and determined the X-ray crystal structures of C*06:02 in the presence of three self-peptides including an analogue of a self-peptide derived from the ADAMTSL5 protein [37]. Thus, we define the HLA-C*06:02 peptide-binding motif and provide the structural basis of peptide selection that will assist in the identification and refinement of psoriasis-related autoantigens.

RESULTS

HLA-C*06:02 Peptide Repertoire

To determine the peptide repertoire and binding motif of HLA-C*06:02, membrane-bound complexes (mC*06:02) were expressed on the surface of the HLA class I-deficient B-cell line 721.221 and peptide complexes purified by immunoaffinity chromatography. Peptides were separated by reverse-phase HPLC and identified by high resolution mass spectrometry. For mC*06:02 a total of 2142 peptides were identified with the peptides predominantly falling in the range of 8–12 amino acids in length (49%) **(Fig. 1*A*).** The most abundant peptide length observed

was nine amino acids with a total of 794 peptides representing 37% of total peptides. Analysis of the nonamer peptides revealed three dominant, conserved residues located at the primary anchor positions P2 and P9 as well as a potential secondary anchor at P7 (**Fig. 1, *B* and *C***). For analysis, cut-offs for dominant, strong, and preferred amino acids were applied at frequencies of >30, >20, and >10%, respectively (as defined previously [40]). At P2, the dominant amino acid was arginine (41%) yet tyrosine (9%) and smaller residues such as alanine (12%), glycine (6%), and serine (6%) were tolerated. The P7 position also showed a clear bias for arginine (40%) and to a lesser extent lysine (12%). The P9 position favored small hydrophobic residues with leucine (40%), valine (25%), and isoleucine (12%) appearing as dominant, strong, and preferred residues, respectively. The P9 position could also accept larger hydrophobic residues such as tyrosine and methionine, however, these occurred at much lower frequencies (9 and 8%, respectively).

The peptide repertoire of a number of HLA-C allomorphs, including HLA-C*06:02, have been previously studied by positional scanning combinatorial peptide libraries (PSCPL) [18]. This method observed a similar motif for HLA-C*06:02 with preferences for a P2-Arg, a small hydrophobic in P9, and a very minor increase in the presence of arginine at P7. The PSCPL screening also indicated that HLA-C*07:01 and HLA-C*07:02 have the closest related peptide motif to HLA-C*06:02 with P2-Arg and P9 hydrophobic anchor residues. Another study was able to ascertain peptide sequences for HLA-C*06:02 from carcinoma cell lines and also showed a similar peptide motif [41]. HLA-C*04:01 is a well-characterized allomorph that has been studied using a similar approach described here for HLA-C*06:02 [19]. HLA-C*04:01 similarly prefers nonamer peptides and terminal hydrophobic anchor residues. The other anchor residues of HLA-C*04:01 are different than HLA-C*06:02 and it prefers a large hydrophobic at P2-(Phe/Tyr) and has a strong preference for aspartic acid at P3 [42].

The peptide repertoire of mC*06:02 also contained peptides ranging from 13 to 23 amino acids in length. These peptides did not conform to a standard peptide motif and did not contain any significant anchor residues. For example, only 2% of peptides of 16 amino acids in length contain a leucine at the terminal position. Therefore, to test the validity of the longer peptides and to confirm our motif, we obtained a peptide repertoire of a soluble form of HLA-C*06:02 (sC*06:02). The use of soluble HLA-I was aimed at reducing the levels of contaminating peptides from cellular lysis and has been used previously to identify naturally processed HLA presented peptides [43–46].

A total of 985 peptides were obtained from sC*06:02. Overall there was a similar length distribution to that of mC*06:02. Nonamers were again the most abundant peptide length (37%) **(Fig. 1A)** and showed significant peptide overlap (60%) with mC*06:02 peptides **(Fig. 1D).** Overall the nonamer peptide motif **(Fig. 1, E and F)** of sC*06:02 was near identical to that of mC*06:02 with only a small difference in the frequency of arginine at P2 (25% as compared with 41%). These minor differences in motif were likely due to the reduced number of peptides obtained from soluble HLA-I, resulting from lower levels of soluble HLA-C expression. The peptide repertoire obtained from sC*06:02 contained a lower proportion of peptides longer than 14 amino acids and a lower number of contaminants. That is, there was a low degree of overlap with the long peptides from mC*06:02 (7%) and there was a greater proportion of longer peptides that had expected residues in the anchor positions. For example, ∼18% of peptides of 16 amino acids in length had leucine at the terminal position. Accordingly, the sC*06:02 provided a means of obtaining a similar peptide repertoire as mC*06:02 with a lower proportion of contaminating peptides.

X-ray crystal structures of HLA-C*06:02

To elucidate the structural basis of HLA-C*06:02-mediated peptide presentation, two HLA-C*06:02 self-peptides, ARTE (ARTELYRSL of Protein_AATF, UniProtKB Q9NY61) and ARFN (ARFNDLRFV of RUNX3, UniProtKB Q13761), were selected from the identified HLA-C*06:02 peptide repertoire. These peptides were selected for meeting the following criteria: (i) they had preferred anchor residues (P2-Arg, P7-Arg, and P9-L/V), (ii) they were consistently identified from peptide elutions, and (iii) they allowed for significant yields of refolded HLA-C*06:02. Furthermore, we selected the previously identified melanocyte peptide antigen ADAMTSL557–65 (VRSRR-abu-LRL) [(37)], where "abu" refers to 2-aminoisobutyric acid, a thiol to methyl-substituted analogue of cysteine. By removing the thiol group, this analogue enabled successful pHLA-I refolding while maintaining T-cell reactivity (data not shown) [(47)]. Refolded HLA-C*06:02 was purified, crystallized, and the structures determined to 1.74 Å for HLA-C*06:02-ARTE, 2.8 Å for HLA-C*06:02-ARFN, and 2.3 Å for HLA-C*06:02-ADAMTSL5 (data collection and refinement statistics are summarized in **Table 1**). The high quality of the data allowed for reliable placement of the peptide ligands **(Fig. 2, A–D).** The ARFN peptide was observed in two conformations that differed in their placement of the P7-Arg (discussed below under "The structure of HLA-C*06:02-ARFN") **(Fig. 2, B and C).**

HLA-C*06:02 adopted the typical MHC class I structure and overall the three crystal structures of HLA-C*06:02 were highly similar (r.m.s. deviations of 0.44–0.76 Å over

residues 1–182). The largest difference was seen in the β1-β2 loop (residues 14–19) of the HLA-C*06:02-ADAMTSL5 with a 7.2 Å shift due to differential crystal packing. A modest difference was seen at the α2 helical-hinge region (residues 147–155), where a 1.2-Å shift in the HLA-C*06:02-ARFN structure was observed due to contacts with the P5 position of the peptide (Fig. 2E). Overlay of the peptides reveals a high degree of similarity, with the greatest differences occurring in the central residues (P4–P7) (Fig. 2F). Nevertheless, the conformation of HLA residues available for interaction with T-cell receptors remain largely conserved.

The structure of HLA-C*06:02-ARTE

Analysis of peptide-ligand binding contacts of the HLA-C*06:02-ARTE structure revealed extensive main chain interactions across the length of the peptide ligand to the HLA molecule. Furthermore, there were internal peptide interactions between the P6-Tyr and P5-Leu, which served to constrain the epitope at these positions [48] **(Fig. 3*A*).** Three peptide side chains were observed to have anchoring roles (P2, P7, and P9), which are buried within the B-, E-, and F-pockets, respectively **(Fig. 3*A*).** The P2-Arg formed main chain hydrogen bonds to Tyr7, Glu63, and Lys66, whereas its side chain was buried deep within the B-pocket and formed salt bridge interactions to Asp9 and a hydrogen bond to Ser24 **(Fig. 3, *A* and *B*).** The P7-Arg was supported via main chain interactions to Gln70 and Asn77, whereas the P7-Arg side chain was buried within the E-pocket where it formed a salt bridge with Asp9 and cation-π stacking against Trp97 **(Fig. 3, *A* and *C*)**. The C-terminal P9-Leu anchor of ARTE is bound within the F-pocket where its backbone and terminal carboxyl formed hydrogen bonds to Asn77, Lys80, Tyr84, and Thr143 **(Fig. 3, *A* and *D*).** The side chain sat in a hydrophobic pocket (Leu81, Tyr123, and Trp147) that helped to stabilize the interaction **(Fig. 3, *A* and *D*).** These extensive interactions at the B-, E-, and F-pockets support the notion of three anchor sites in HLA-C*06:02 with the salt-bridging interactions at the B- and E-pockets correlating with the observed preference for arginine anchors at these positions within the peptide repertoire studies.

The structure of HLA-C*06:02-ARFN

Although the overall tertiary structure of HLA-C*06:02-ARFN was similar to that of C*06:02-ARTE, the ARFN peptide was nonetheless observed in two conformations that differed in the orientations of the P7-Arg **(Fig. 2, *B, C,* and *F*)** (discussed below). The ARFN peptide displayed internal constraints between P3-Phe and P5-Asp **(Fig. 2, *B, C,* and *F*).** Yet, overall the four ARFN peptide copies in the asymmetric unit were highly similar to each other at the P3 and P5 positions

and to each other and the ARTE structure, detailed above, at the P2 and P9 anchor positions. That is, the P2-Arg residues formed backbone contacts to Tyr7, Glu63, and Lys66 and the side chains were buried within the B-pocket where they made contacts to the Ser24 and Asp9 residues **(Fig. 4*A*)**. The P9-V was buried in the F-pocket and formed equivalent backbone contacts (Asn77, Tyr84, and Thr143) and hydrophobic side chain contacts to Leu81, Tyr123, and Trp147 **(Fig. 4*B*).** Thus, whereas the P7-Arg in ARFN adopted two distinct conformations within the crystal, this was not clearly attributable to alterations within the peptide or peptide-binding groove distal to the E pocket. One P7-Arg conformation (ARFN-1) was in a conformation similar to that observed in ARTE with the side chain forming a salt bridge interaction with Asp9 and cation-π interactions with Trp97 **(Fig. 4*C*)**. In the other P7-Arg conformation (ARFN-2) the P7-Arg side chain shifted 5.8 Å and no longer formed a salt bridge with Asp9, but instead formed a salt bridge with Asp114 **(Fig. 4*C*).** Although the conformation of E-pocket residues was conserved within the ARFN structures, there was a 140° rotation of Trp97 between ARTE and ARFN **(Fig. 4*D*).** Taken together, it is likely that plasticity of Trp97 in the E-pocket of HLA-C*06:02 fosters changes in the microenvironment around P7-Arg anchors such that they can form alternate salt-bridge partners with Asp9 or Asp114.

X-ray crystal structure HLA-C*06:02 with an analogue of a melanocyte peptide antigen (ADAMTSL5)

To structurally characterize the presentation of the melanocyte peptide antigen ADAMTSL5 (VRSRRCLRL) by HLA-C*06:02 we refolded HLA-C*06:02 with an ADAMTSL5 analogue (VRSRR-abu-LRL) that has aminobutyric acid in place of the P6-Cys. This synthetic analogue of cysteine was necessary for successful *in vitro* refolding of the complex for crystallization. Crystals of HLA-C*06:02 in complex with the ADAMTSL5 analogue were obtained and a structure solved to 2.3 Å (data collection and refinement statistics are summarized in Table 1).

The X-ray crystal structure revealed very similar interactions for the P2-Arg and P9-Leu as seen in structures of both ARTE and ARFN complexes **(Fig. 5*A*).** Instead of a P7-Arg, however, the ADAMTSL5 had a P7-Leu. Although not a dominant residue preference, P7-Leu was present in ~4% of nonamers eluted from cellular HLA-C*06:02 molecules. The P7-Leu side chain is buried within the E-pocket where it forms hydrophobic interactions with Trp97. Of note, Trp97 adopts a conformation distinct to that observed in the ARTE and ARFN structures with a 114° rotation **(Fig. 5*B*)**. Thus, whereas there was significant conservation of HLA residue conformations in regions that are available to T-cell receptor recognition, there was plasticity of the Trp97 side chain to facilitate different conformations and residues within the E-pocket of HLA-C*06:02.

Structural and sequence similarities of HLA-C allomorphs

There is currently a relative lack of structural information for HLA-C with only 5 allomorphs available in the PDB, C*08:01 [49], C*04:01 [50], C*05:01 [51], C*07:02 [51], and C*03:04 [52]. Comparison of our highest resolution HLA-C*06:02 structure (ARTE) to the other currently available HLA-C structures revealed a high degree of similarity of the peptide-binding grooves with r.m.s. deviations over residues 1–182 of 0.75 Å to HLA-C*08:01 (4NT6), 0.71 Å to C*03:04 (1EFX), 0.97 Å to C*05:01, 0.68 Å to C*07:02 and 0.81 Å to C*04:01 (1QQD). Comparison of HLA-C*06:02-ARTE to HLA-B27:05, an allomorph that also has a preference for peptides with a P2-Arg [42], also showed a high degree of similarity in the peptide-binding groove, with an r.m.s. deviation of 0.63 **(Fig. 6*A*).**

The surface electrostatics of HLA-C*06:02 reveals a primarily negative charge across the peptide-binding groove, especially in the B- and E-pockets **(Fig. 6*B*).** By contrast, the other available HLA-C structures have more positively charged peptide-binding grooves **(Fig. 6, *A*–*G*).** HLA-C*04:01 has a highly positive B-pocket and small area of negative charge in the E-pocket **(Fig. 6*C*),** whereas C*03:04 has a similarly negatively charged E-pocket, yet a relatively uncharged B-pocket **(Fig. 6*D*)**, and in contrast HLA-C*05:01 and HLA-C*08:01 have mostly positively charged B- and E-pockets **(Fig. 6, *E*and *F*).** On the other hand HLA-C*07:02 and HLA-B*27:05, both allomorphs that have a preference for peptides with a P2-Arg [42, 51], also display a high degree of negative charges across the entire peptide-binding groove **(Fig. 6, *G* and *H*).** Analysis of the peptide-binding pocket volume with the CASTp server [53] shows HLA-C*06:02-ARTE has a much larger binding pocket than the other available HLA-C structures. HLA-C*06:02 has a pocket volume of 1900 Å3, whereas the other available HLA-C structures range between 1600 and 1800 Å3. This large volume for HLA-C*06:02 is attributable to the deep B- and E-binding pockets.

HLA-C*04:01 is a relatively well-understood HLA-C allomorph with a previously published peptide repertoire and a crystal structure available (PDB 1QQD) (19, 50). Accordingly, HLA-C*04:01 was selected to provide a structural comparison with HLA-C*06:02. A sequence alignment of the B- and E-pockets of some of the common HLA-C allomorphs reveals that most of the HLA-C allomorphs lack the necessary residues for positively charged anchor residues at P2 and P7 **(Fig. 7*A*).** In the B-pocket, the majority of the HLA-C allomorphs lack the negatively charged Asp9 that attracts positively charged P2 anchor residues. Indeed, the only allomorphs that have a Asp9 are the HLA-Cw6 and HLA-Cw7 allomorphs that have similarly been shown to present peptides with P2-Arg (18). From a structural perspective, the allomorphic differences in HLA-

C*04:01 are evident. Namely, HLA-C*04:01 lacks the necessary negatively charged B-pocket and instead has a B-pocket with small uncharged residues (Ser9 and Ala24) and has a preference for large hydrophobic residues such as phenylalanine or tyrosine **(Fig. 7, *B* and *C*).** In the E-pocket, positions 114 and 97 are dimorphic (Asn to Asp and Arg to Trp, respectively) so that they are unlikely to prefer positively charged P7 anchor residues **(Fig. 7*A*).** For example, in HLA-C*04:01, residues 97 and 156 are Arg (as opposed to Trp in C*06:02), and thus would repel positively charged peptide residues **(Fig. 7, *D* and *E*).** In the F-pocket, the majority of pocket residues are conserved and therefore they are likely to have similar hydrophobic residue terminal anchor preferences **(Fig. 7, *A*, *F*, and *G*).** Interestingly, the only other common HLA-C allomorph with an E-pocket strictly conserved with HLA-C*06:02 is C*12:03, which has tentative associations with psoriasis and psoriasis arthritis [54, 55]. Accordingly, HLA-C*06:02 has a unique peptide-binding groove with very negatively charged B- and E-pockets, making it well-suited to bind peptides containing large positive charged residues at the P2 and P7 positions, and thus selects a unique repertoire of peptides.

DISCUSSION

The HLA-C*06:02 peptide repertoire data provides important new insights into determinant selection by this molecule. For instance, HLA-C*06:02 peptides have been previously eluted from cancer cell lines in the presence of other HLA allomorphs [41], whereas another study utilized non-native peptide libraries as a general approach for studying HLA-C peptide motifs including C*06:02 [18]. These studies are in general agreement with our findings that HLA-C*06:02 prefers nonamer peptides and has strong preferences for Arg and Leu at P2 and PΩ, respectively. By contrast, the preference for the P7-arginine, although observed in previous studies occurred at a low frequency [18, 41]. Our data suggests that the P7-arginine occurs at similar frequencies to the P2-arginine and is likely an equally dominant anchor residue. This discrepancy is likely due to the improved robustness of our dataset imparted by the elution of a larger number of peptides and the elution of naturally presented self-peptides. The presence of longer peptides (14–18-mers) in our dataset was unexpected. As we have accounted for common HLA-II-associated contaminants, and the longer peptides do not conform to the motif we defined for HLA-C*06:02, we suspect these longer peptides are contaminants from other cellular sources. Yet, we cannot rule out that there may be *bona fide* epitopes within this longer subset.

The preference for Arg at P2 and P7 appears to be a unique feature, among the common HLA-C alleles, of HLA-C*06:02. Peptide repertoire analysis allowed us to identify peptides with optimal anchor residues for HLA-C*06:02. From these peptides we identified ARTE (ARTELYRSL, UniProtKB Q9NY61) and ARFN (ARFNDLRFV of RUNX3, UniProtKB Q13761) for which we were able to determine structures bound to HLA-C*06:02. In line with the peptide repertoire data, these structures reveal that HLA-C*06:02 has two deep electronegative pockets that prefer the accommodation of P2- and P7-arginine residues. The E-pocket of HLA-C*06:02 has a mobile Trp97 residue, which allows for multiple orientations of the P7-Arg of the presented peptides. From sequence alignments and previous repertoire data [18] it can be seen that other HLA-C allomorphs have Arg preferences at P2 or P7, but no other common allotype has both. For example, the HLA-Cw7 group has preference for P2-Arg containing peptides and HLA-C*12:03 likely has a preference for an Arg at P7 [18]. This preference for a P7-Arg coincides with a tentative association of HLA-C*12:03 with psoriasis [54]. Thus, HLA-C*06:02 has a uniquely negatively charged antigen-binding cleft that inclines the molecule to the presentation of a distinct repertoire of positively charged peptides.

Using this repertoire-determined motif we are able to predict the ability of putative peptide antigens to be presented by HLA-C*06:02. To date, a number of putative HLA-C*06:02-restricted psoriasis peptide antigens have been identified, including peptides from: streptococcus M protein, human keratin, the antimicrobial LL-37 and recently a peptide antigen from melanocytes. We can collate the current putative HLA-C*06:02-restricted peptide antigens and rank their potential to be presented by HLA-C*06:02 **(Table 2).** Based on these predictions the streptococcus M6 peptides 282M6–9 and 324M6–9 have a high likelihood of being presented by HLA-C*06:02 because both of these peptides have the preferred P2- and P7-Arg residues and the terminal P9-Leu [56]. Most of the identified Keratin17 peptides will likely have low association with HLA-C*06:02 with the exception of 217K17–9, which has the preferred P7-Arg and P9-Leu. Similarly, for the LL-37 peptides identified most are predicted to associate poorly with HLA-C*06:02 with the exception of the LL37p6s and LL37p5s peptides [36] **(Table 2)**. Indeed, of the LL-37 epitopes predicted by *in silico* methods to bind HLA-C*06:02 we were only able to successfully refold LL37p6s and LL37p5s (data not shown). Accordingly, this structurally-informed peptide repertoire analysis provides a template to rank the affinity of putative psoriatic autoantigens for HLA-C*06:02.

The HLA-C*06:02–VRSRR-abu-LRL structure suggests that the mimotopes identified by Arakawa *et al.* [37] share a common positively charged solvent-accessible surface for docking of the

Vα3S1/Vβ13S1 TCR. The Vα3S1/Vβ13S1 TCR was previously identified from a CD8+ T-cell clone isolated from the epidermis of lesional skin tissue of a HLA-C*06:02-positive psoriasis patient [37, 57]. A preference for Vβ13.1 gene usage has been seen previously in epidermal psoriatic CD8+ T-cells [58, 59]. As the VRSRR-abu-LRL peptide had canonical P2-Arg and P9-Leu anchors with the leucine in the P7 position accommodated by reorientation of the Trp97, the trio of arginine residues at P4, P5, and P8 are solvent exposed. This trio of arginines is highly conserved in mimotopes recognized by the Vα3S1/Vβ13S1 TCR, suggesting it is the positively charged surface of the epitope that promotes TCR recognition [37]. However, the extent to which the Va3S1/Vb13S1 TCR and the ADAMTSL5 peptide are a *bona fide*psoriatic autoreactive pairing is unknown as the trigger(s) of psoriasis remain unclear. Furthermore, the extent to which Vβ13.1 gene usage is a general feature of psoriatic TCR repertoires is unknown. Nonetheless, it is tempting to speculate that arginine- and lysine-rich epitopes on antimicrobial peptides or bacterial proteins (like streptococcal M protein) may elicit HLA-C*06:02 restricted autoreactivity. In conclusion, in presenting the peptide repertoire and structural characterization of HLA-C*06:02 we provide a base for further rational interrogation of this molecule.

EXPERIMENTAL PROCEDURES

Cell line development and culture

Full-length HLA-C*06:02 was cloned into the pcDNA3.1 vector and stably transfected into the HLA class Ia-deficient cell line 721.221 by antibiotic selection. The full-length HLA-C*06:02 721.221 cell line (mC*06:02) was cultured in RPMI 1640 supplemented with 10% FCS, 1× GlutaMAX (Gibco), and G418 sulfate (50 μg/ml).

HLA-C*06:02 was truncated to create a soluble construct that lacked the transmembrane and cytoplasmic regions (residues 1–303). The soluble construct was cloned into the pIRES2-ZsGreen1 vector and transfected into the 721.221 cell line by Lipofectamine 2000 reagent and standard protocols. Cell lines were selected with G418 sulfate antibiotic and sorted by GFP expression levels at FlowCore (Monash University). The soluble C*06:02 721.221 cell line (sC*06:02) was cultured in CELLine bioreactor flasks (Argos Technologies) with RPMI 1640 media supplemented with 2% FCS, 1× GlutaMAX (Gibco), and G418 sulfate (50 μg/ml).

Peptide repertoire by mass spectrometry

The peptide repertoire of full-length HLA-C*06:02 *(*mC*06:02) was determined as previously described (19). In short, 3 × 109 721.221 cells were lysed by cryogenic grinding in a Mixer Mill MM 400 (Retsch) followed by incubation in 50 mM Tris, pH 8.0, 150 mM NaCl, 2.5 mM EDTA, 0.5% IGEPAL (Sigma) and protease inhibitors (Roche Applied Science) and mC*06:02 was purified using the Pan-HLA class I antibody W6/32 immobilized to protein A resin. HLA-protein complexes were eluted with 10% acetic acid and peptides were further separated by reverse-phase HPLC. Peptides were then analyzed by Q Exactive Hybrid Quadrupole-Orbitrap Mass Spectrometer (Thermo Scientific) and identified by database search using the human UniProtKB/SwissProt database (Feb 2016) [(60)] with ProteinPilot version 5.0 (SCIEX). A false discovery rate of 5% was applied and a list of known contaminants, including known class II peptide ligands derived from this cell line, removed. The peptide repertoire of soluble HLA-C*06:02 (sC*06:02) was determined as described for membrane-bound HLA-C*06:02 with the exception that the initial cellular lysis steps were omitted and sC*06:02 was immunoaffinity purified directly from the cell culture media. A list of identified peptides is shown in supplemental **Table S1**.

Protein expression and purification

The extracellular portion of HLA-C*06:02 (residues 1–274) and human β2-microglobulin (β2m) were each cloned into the pET30 expression vector system and expressed into inclusion bodies within Escherichia coli. Inclusion bodies were harvested and solubilized in 20 mM Tris-HCl, pH 8.0, 6 M guanidine hydrochloride, 1 mM EDTA, 1 mM DTT, and 0.2 mM PMSF. HLA-C*06:02 heavy chain was refolded in the presence of human β2m (120 and 30 mg, respectively) and 10 mg of the self-peptides ARTE (ARTELYRSL of Protein_AATF, UniProtKB Q9NY61) or ARFN (ARFNDLRFV of RUNX3, UniProtKB Q13761) or an analogue of a melanocyte autoantigen (VRSRR-abu-LRL of ADAMTSL5, UniProtKB X6R4H8), where an aminobutyric acid residue is substituted in place of cysteine in the P6 position [(37)]. Refolds were carried out in 1 liter of refold buffer (0.1 M Tris-HCl, pH 8.0, 2 mM EDTA, 0.4 M L-arginine, 0.5 mM oxidized glutathione, 5 mM reduced glutathione, and 0.2 mM PMSF). The refold solution was then dialyzed into 20 mM Tris-HCl, pH 8.0. Refolded HLA-C*06:02 was initially purified by weak anion exchange (DEAE-Sepharose) followed by size exclusion chromatography on a S200/16/60 column (GE Healthcare) in 20 mM Tris, pH 8.0, 150 mM NaCl. The final purification step was anion exchange chromatography with a HiTrap Q column with a linear gradient of 20 mM Tris, pH 8.0, 0 to 1 M NaCl. Samples were buffer exchanged to 20 mM Tris, pH 8.0, 150 mM NaCl for storage prior to use.

Crystallization and X-ray data collection

Prior to crystallization HLA-C*06:02 was concentrated to 10 mg/ml in a buffer comprised of 10 mM Tris, pH 8.0, 100 mM NaCl. Crystals of HLA-C*06:02 were grown using the hanging-drop vapor diffusion method at 298 K. The HLA-C*06:02-ARTE crystals were grown from a reservoir solution of 0.1 M Bis-Tris propane, pH 7.0, 0.1 Msodium fluoride, and 20% PEG 8000. The HLA-C*06:02-ARFN crystals were grown in 0.1 M Tris, pH 8.5, 0.2 M sodium acetate, and 20% PEG 3350. HLA-C6*06:02-ADAMTSL5 crystals were grown from a reservoir solution of 0.1 M sodium acetate, pH 4.5, and 1.8 M ammonium citrate. Crystals were equilibrated in reservoir solution with the addition of 15% sucrose for HLA-C*06:02-ARTE and 30% PEG 3350 for HLA-C*06:02-ARFN and 15% ethylene glycol for HLA-C*06:02-ADAMTSL5 prior to flash cooling in liquid nitrogen for data collection. X-ray diffraction were collected at 100 K at the MX2 beamline of the Australian Synchrotron.

Structure determination and refinement

X-ray crystal images were processed with XDS [(61)] and then scaled and merged with AIMLESS [(62)]. For HLA-C*06:02-ARTE initial phases were solved by molecular replacement using PHASER [(63)] with HLA-C*08:01 used as the initial search model (PDB 4NT6) [(49)]. An initial round of rigid body refinement was carried out with REFMAC5 [(64)], followed by rounds of restrained refinement in REFMAC5 and model building with COOT [(65)]. Solvent was added with ARP/wARP [(66)]. Translational liberation screw rotation (TLS) refinement was applied to the final rounds of refinement in REFMAC. Initial phases of HLA-C*06:02-ARFN were solved using PHASER with HLA-C*06:02-ARTE (excluding the peptide ligand) as the initial search model. Repeated rounds of refinement were carried out with BUSTER [(67)] and model building with COOT. NCS restraints were applied and TLS refinement was applied in final rounds of refinement.

Initial phases of HLA-C*06:02-ADAMTLS5 were also determined using HLA-C*06:02-ARTE without the peptide ligand as the search model as implemented in PHASER. Iterative rounds of refinement were carried out with PHENIX [(68)] and model building with COOT. A single round of simulated annealing was performed to minimize bias and TLS was applied to final rounds of refinement.

HLA-C*06:02-ARTE was solved in the P21 space group and refined to a resolution of 1.74 Å. The final structure contained two HLA-C*06:02 protein complexes in the asymmetric unit with each comprising residues 2–274 of HLA-C*06:02 heavy chain and the full-length β2m (1–99) as well as

an additional N-terminal start methionine (M0). The entire ARTE peptide (ARTELYRSL) was visible for both complexes and unambiguously built.

HLA-C*06:02-ARFN was solved in the P212121 space group at 2.8-Å resolution. The structure contained four HLA-C*06:02 protein complexes in the asymmetric unit. Three HLA-C*06:02 protein complexes were comprised of residues 2–274 for the heavy chain, with one chain lacking residues 104–108 of the α2S1-S2 loop. All protein complexes comprised full-length β2m (0–99) and had unambiguous density for the ARFN peptide (ARFNDLRFV).

HLA-C*06:02-ADAMTSL5 was also solved in the P212121 space group to a resolution of 2.3 Å and contained one HLA-C*06:02 protein complex in the asymmetric unit. The protein complex comprised residues 2–274 for the heavy chain and residues 1–99 for β2m. The peptide ligand (VRSRR-abu-LRL) had clear density for all side chain atoms with the exception of the P4-Arg, which had insufficient density beyond atom Cδ. The P6 aminobutyric acid residue was built using ABA from the CCP4 monomer library. Data collection and refinement statistics for all structures are summarized in Table 1.

Abbreviations used:

HLA	human leukocyte antigen
KIR	Killer-cell immunoglobulin-like receptors
ARTE	ARTELYRSL
r.m.s.	root mean square
PSORS1	psoriasis susceptibility locus 1
β2m	β2-microglobulin
abu	aminobutyric acid
Bis-Tris propane	1,3-bis[tris(hydroxymethyl)methylamino]propane
TLS	translational liberation screw rotation
PDB	Protein Data Bank.

REFERENCES

1. Parham, P. (2005) MHC class I molecules and KIRs in human history, health and survival. Nat Rev Immunol 5, 201-214

2. Saunders, P. M., Vivian, J. P., O'Connor, G. M., Sullivan, L. C., Pymm, P., Rossjohn, ., and Brooks, A. G. (2015) A bird's eye view of NK cell receptor interactions with their MHC clss I ligands. Immunol Rev 267, 148-166

3. Rossjohn, J., Gras, S., Miles, J. J., Turner, S. J., Godfrey, D. I., and McCluskey, J. (2015) T cell antigen receptor recognition of antigen-presenting molecules. Annu Rev Immunol 33, 169-200

4. Archbold, J. K., Macdonald, W. A., Gras, S., Ely, L. K., Miles, J. J., Bell, M. J., Brennan, R. M., Beddoe, T., Wilce, M. C., Clements, C. S., Purcell, A. W., McCluskey, J., Burrows, S. R., and Rossjohn, J. (2009) Natural micropolymorphism in human leukocyte antigens provides a basis for genetic control of antigen recognition. J Exp Med 206, 209-219

5. Garboczi, D. N., Ghosh, P., Utz, U., Fan, Q. R., Biddison, W. E., and Wiley, D. C. (1996) Structure of the complex between human T-cell receptor, viral peptide and HLA-A2. Nature 384, 134-141

6. Parham, P., Adams, E. J., and Arnett, K. L. (1995) The origins of HLA-A,B,C polymorphism. Immunol Rev 143, 141-180

7. Illing, P. T., Vivian, J. P., Dudek, N. L., Kostenko, L., Chen, Z., Bharadwaj, M., Miles, J. J., Kjer-Nielsen, L., Gras, S., Williamson, N. A., Burrows, S. R., Purcell, A. W., Rossjohn, J., and McCluskey, J. (2012) Immune self-reactivity triggered by drugmodified HLA-peptide repertoire. Nature 486, 554-558

8. Minos, E., Barry, R. J., Southworth, S., Folkard, A., Murray, P. I., Duker, J. S., Keane, P. A., and Denniston, A. K. (2016) Birdshot chorioretinopathy: current knowledge and new concepts in pathophysiology, diagnosis, monitoring and treatment. Orphanet J Rare Dis 11, 61

9. Chen, B., Li, J., He, C., Li, D., Tong, W., Zou, Y., and Xu, W. (2017) Role of HLA-B27 in the pathogenesis of ankylosing spondylitis (Review). Mol Med Rep

10. Nair, R. P., Stuart, P. E., Nistor, I., Hiremagalore, R., Chia, N. V., Jenisch, S., Weichenthal, M., Abecasis, G. R., Lim, H. W., Christophers, E., Voorhees, J. J., and Elder, J. T. (2006) Sequence and haplotype analysis supports HLA-C as the psoriasis susceptibility 1 gene. Am J Hum Genet 78, 827-851

11. Dudek, N. L., and Purcell, A. W. (2014) The beta cell immunopeptidome. Vitam Horm 95, 115-144

12. McGinty, J. W., Marre, M. L., Bajzik, V., Piganelli, J. D., and James, E. A. (2015) T cell epitopes and post-translationally modified epitopes in type 1 diabetes. Curr Diab Rep 15, 90

13. Scally, S. W., Petersen, J., Law, S. C., Dudek, N. L., Nel, H. J., Loh, K. L., Wijeyewickrema, L. C., Eckle, S. B., van Heemst, J., Pike, R. N., McCluskey, J., Toes, R. E., La Gruta, N. L., Purcell, A. W., Reid, H. H., Thomas, R., and Rossjohn, J. (2013) A molecular basis for the association of the HLA-DRB1 locus, citrullination, and rheumatoid arthritis. J Exp Med 210, 2569-2582

14. van Gaalen, F. A., van Aken, J., Huizinga, T. W., Schreuder, G. M., Breedveld, F. C., Zanelli, E., van Venrooij, W. J., Verweij, C. L., Toes, R. E., and de Vries, R. R. (2004) Association between HLA class II genes and autoantibodies to cyclic citrullinated peptides (CCPs) influences the severity of rheumatoid arthritis. Arthritis Rheum 50, 2113-2121

15. Petersen, J., Montserrat, V., Mujico, J. R., Loh, K. L., Beringer, D. X., van Lummel, M., Thompson, A., Mearin, M. L., Schweizer, J., Kooy-Winkelaar, Y., van Bergen, J., Drijfhout, J. W., Kan, W. T., La Gruta, N. L., Anderson, R. P., Reid, H. H., Koning, F., and Rossjohn, J. (2014) T-cell receptor recognition of HLA-DQ2-gliadin complexes associated with celiac disease. Nat Struct Mol Biol 21, 480-488

16. Henderson, K. N., Tye-Din, J. A., Reid, H. H., Chen, Z., Borg, N. A., Beissbarth, T., Tatham, A., Mannering, S. I., Purcell, A. W., Dudek, N. L., van Heel, D. A., McCluskey, J., Rossjohn, J., and Anderson, R. P. (2007) A structural and immunological basis for the role of human leukocyte antigen DQ8 in celiac disease. Immunity 27, 23-34

17. Kim, C. Y., Quarsten, H., Bergseng, E., Khosla, C., and Sollid, L. M. (2004)Structural basis for HLA-DQ2-mediated presentation of gluten epitopes in celiacdisease. Proc Natl Acad Sci U S A 101, 4175-4179

18. Rasmussen, M., Harndahl, M., Stryhn, A., Boucherma, R., Nielsen, L. L., Lemonnier, F. A., Nielsen, M., and Buus, S. (2014) Uncovering the peptide-binding specificities of HLA-C: a general strategy to determine the specificity of any MHC class I molecule. J Immunol 193, 4790-4802

19. Schittenhelm, R. B., Dudek, N. L., Croft, N. P., Ramarathinam, S. H., and Purcell, A. W. (2014) A comprehensive analysis of constitutive naturally processed and presented HLA-C*04:01 (Cw4)-specific peptides. Tissue Antigens 83, 174-179

20. Kaur, G., Gras, S., Mobbs, J. I., Vivian, J. P., Cortes, A., Barber, T., Kuttikkatte, S. B., Jensen, L. T., Attfield, K. E., Dendrou, C. A., Carrington, M., McVean, G., Purcell, A. W., Rossjohn, J., and Fugger, L. (2017) Structural and regulatory diversity shape HLA-C protein expression levels. Nat Commun 8, 15924

21. Vita, R., Overton, J. A., Greenbaum, J. A., Ponomarenko, J., Clark, J. D., Cantrell, J. R., Wheeler, D. K., Gabbard, J. L., Hix, D., Sette, A., and Peters, B. (2015) The immune epitope database (IEDB) 3.0. Nucleic Acids Res 43, D405-412

22. Berman, H. M., Westbrook, J., Feng, Z., Gilliland, G., Bhat, T. N., Weissig, H., Shindyalov, I. N., and Bourne, P. E. (2000) The Protein Data Bank. Nucleic Acids Res 28, 235-242

23. McCutcheon, J. A., Gumperz, J., Smith, K. D., Lutz, C. T., and Parham, P. (1995) Low HLA-C expression at cell surfaces correlates with increased turnover of heavy chain mRNA. J Exp Med 181, 2085-2095

24. Snary, D., Barnstable, C. J., Bodmer, W. F., and Crumpton, M. J. (1977) Molecular structure of human histocompatibility antigens: the HLA-C series. Eur J Immunol 7,580-585

25. Blais, M. E., Dong, T., and Rowland-Jones, S. (2011) HLA-C as a mediator of natural killer and T-cell activation: spectator or key player? Immunology 133, 1-7

26. Harden, J. L., Krueger, J. G., and Bowcock, A. M. (2015) The immunogenetics of Psoriasis: A comprehensive review. J Autoimmun 64, 66-73

27. Gudjonsson, J. E., Karason, A., Antonsdottir, A., Runarsdottir, E. H., Hauksson, V. B., Upmanyu, R., Gulcher, J., Stefansson, K., and Valdimarsson, H. (2003) Psoriasis patients who are homozygous for the HLA-Cw*0602 allele have a 2.5-fold increased risk of developing psoriasis compared with Cw6 heterozygotes. Br J Dermatol 148, 233-235

28. Henseler, T., and Christophers, E. (1985) Psoriasis of early and late onset: characterization of two types of psoriasis vulgaris. J Am Acad Dermatol 13, 450-456

29. Dunphy, S. E., Sweeney, C. M., Kelly, G., Tobin, A. M., Kirby, B., and Gardiner, C. M. (2015) Natural killer cells from psoriasis vulgaris patients have reduced levels of cytotoxicity associated degranulation and cytokine production. Clin Immunol

30. Luszczek, W., Manczak, M., Cislo, M., Nockowski, P., Wisniewski, A., Jasek, M., and Kusnierczyk, P. (2004) Gene for the activating natural killer cell receptor, KIR2DS1, is associated with susceptibility to psoriasis vulgaris. Hum Immunol 65, 758-766

31. Martin, M. P., Nelson, G., Lee, J. H., Pellett, F., Gao, X., Wade, J., Wilson, M. J., Trowsdale, J., Gladman, D., and Carrington, M. (2002) Cutting edge: susceptibility to psoriatic arthritis: influence of activating killer Ig-like receptor genes in the absence of specific HLA-C alleles. J Immunol 169, 2818-2822

32. Cai, Y., Fleming, C., and Yan, J. (2012) New insights of T cells in the pathogenesis of psoriasis. Cell Mol Immunol 9, 302-309

33. Di Cesare, A., Di Meglio, P., and Nestle, F. O. (2009) The IL-23/Th17 axis in the immunopathogenesis of psoriasis. J Invest Dermatol 129, 1339-1350

34. Vollmer, S., Menssen, A., and Prinz, J. C. (2001) Dominant lesional T cell receptor rearrangements persist in relapsing psoriasis but are absent from nonlesional skin: evidence for a stable antigen-specific pathogenic T cell response in psoriasis vulgaris. J Invest Dermatol 117, 1296-1301

35. Valdimarsson, H., Thorleifsdottir, R. H., Sigurdardottir, S. L., Gudjonsson, J. E., and Johnston, A. (2009) Psoriasis--as an autoimmune disease caused by molecular mimicry. Trends Immunol 30, 494-501

36. Lande, R., Botti, E., Jandus, C., Dojcinovic, D., Fanelli, G., Conrad, C., Chamilos, G., Feldmeyer, L., Marinari, B., Chon, S., Vence, L., Riccieri, V., Guillaume, P., Navarini, A. A., Romero, P., Costanzo, A., Piccolella, E., Gilliet, M., and Frasca, L. (2014) The antimicrobial peptide LL37 is a T-cell autoantigen in psoriasis. Nat Commun 5, 5621

37. Arakawa, A., Siewert, K., Stohr, J., Besgen, P., Kim, S. M., Ruhl, G., Nickel, J., Vollmer, S., Thomas, P., Krebs, S., Pinkert, S., Spannagl, M., Held, K., Kammerbauer, C., Besch, R., Dornmair, K., and Prinz, J. C. (2015) Melanocyte antigen triggers autoimmunity in human psoriasis. J Exp Med 212, 2203-2212

38. McFadden, J., Valdimarsson, H., and Fry, L. (1991) Cross-reactivity between streptococcal M surface antigen and human skin. Br J Dermatol 125, 443-447

39. Gudmundsdottir, A. S., Sigmundsdottir, H., Sigurgeirsson, B., Good, M. F., Valdimarsson, H., and Jonsdottir, I. (1999) Is an epitope on keratin 17 a major target for autoreactive T lymphocytes in psoriasis? Clin Exp Immunol 117, 580-586

40. Falk, K., Rotzschke, O., Stevanovic, S., Jung, G., and Rammensee, H. G. (1991) Allele-specific motifs revealed by sequencing of self-peptides eluted from MHC molecules. Nature 351, 290-296

41. Bassani-Sternberg, M., Pletscher-Frankild, S., Jensen, L. J., and Mann, M. (2015) Mass spectrometry of human leukocyte antigen class I peptidomes reveals strong effects of protein abundance and turnover on antigen presentation. Mol Cell Proteomics 14, 658-673

42. Schittenhelm, R. B., Sian, T. C., Wilmann, P. G., Dudek, N. L., and Purcell, A. W. (2015) Revisiting the arthritogenic peptide theory: quantitative not qualitative changes in the peptide repertoire of HLA-B27 allotypes. Arthritis Rheumatol 67, 702-713

43. Kunze-Schumacher, H., Blasczyk, R., and Bade-Doeding, C. (2014) Soluble HLA technology as a strategy to evaluate the impact of HLA mismatches. J Immunol Res 2014, 246171

44. Badrinath, S., Saunders, P., Huyton, T., Aufderbeck, S., Hiller, O., Blasczyk, R., and Bade-Doeding, C. (2012) Position 156 influences the peptide repertoire and tapasin dependency of human leukocyte antigen B*44 allotypes. Haematologica 97, 98-106

45. Scull, K. E., Dudek, N. L., Corbett, A. J., Ramarathinam, S. H., Gorasia, D. G.,Williamson, N. A., and Purcell, A. W. (2012) Secreted HLA recapitulates the immunopeptidome and allows in-depth coverage of HLA A*02:01 ligands. Mol Immunol 51, 136-142

46. Kraemer, T., Celik, A. A., Huyton, T., Kunze-Schumacher, H., Blasczyk, R., and Bade-Doding, C. (2015) HLA-E: Presentation of a Broader Peptide Repertoire Impacts the Cellular Immune Response-Implications on HSCT Outcome. Stem Cells Int 2015, 346714

47. Webb, A. I., Dunstone, M. A., Chen, W., Aguilar, M. I., Chen, Q., Jackson, H., Chang, L., Kjer-Nielsen, L., Beddoe, T., McCluskey, J., Rossjohn, J., and Purcell, A. W. (2004) Functional and structural characteristics of NY-ESO-1-related HLA A2-restricted epitopes and the design of a novel immunogenic analogue. J Biol Chem 279, 23438-23446

48. Theodossis, A., Guillonneau, C., Welland, A., Ely, L. K., Clements, C. S., Williamson, N. A., Webb, A. I., Wilce, J. A., Mulder, R. J., Dunstone, M. A., Doherty, P. C., McCluskey, J., Purcell, A. W., Turner, S. J., and Rossjohn, J. (2010) Constraints within major histocompatibility complex class I restricted peptides: presentation and consequences for T-cell recognition. Proc Natl Acad Sci U S A 107, 5534-5539

49. Choo, J. A., Liu, J., Toh, X., Grotenbreg, G. M., and Ren, E. C. (2014) The immunodominant influenza A virus M158-66 cytotoxic T lymphocyte epitope exhibits degenerate class I major histocompatibility complex restriction in humans. J Virol 88, 10613-10623

50. Fan, Q. R., and Wiley, D. C. (1999) Structure of human histocompatibility leukocyte antigen (HLA)-Cw4, a ligand for the KIR2D natural killer cell inhibitory receptor. J Exp Med 190, 113-123

51. Kaur, G., Gras, S., Mobbs, J. I., Vivian, J. P., Cortes, A., Barber, T., Kuttikkatte, S. B., Jensen, L. T., Attfield, K. E., Dendrou, C. A., Carrington, M., McVean, G., Purcell, A. W., Rossjohn, J., and Fugger,

L. (2017) Structural and regulatory diversity shape HLA-C protein expression levels. Nature Communications 8, ncomms15924

52. Boyington, J. C., Motyka, S. A., Schuck, P., Brooks, A. G., and Sun, P. D. (2000) Crystal structure of an NK cell immunoglobulin-like receptor in complex with its class I MHC ligand. Nature 405, 537-543

53. Dundas, J., Ouyang, Z., Tseng, J., Binkowski, A., Turpaz, Y., and Liang, J. (2006) CASTp: computed atlas of surface topography of proteins with structural and topographical mapping of functionally annotated residues. Nucleic Acids Res 34, W116-118

54. Okada, Y., Han, B., Tsoi, L. C., Stuart, P. E., Ellinghaus, E., Tejasvi, T., Chandran, V., Pellett, F., Pollock, R., Bowcock, A. M., Krueger, G. G., Weichenthal, M., Voorhees, J. J., Rahman, P., Gregersen, P. K., Franke, A., Nair, R. P., Abecasis, G. R., Gladman, D. D., Elder, J. T., de Bakker, P. I., and Raychaudhuri, S. (2014) Fine mapping major histocompatibility complex associations in psoriasis and its clinical subtypes. Am J Hum Genet 95, 162-172

55. Winchester, R., Minevich, G., Steshenko, V., Kirby, B., Kane, D., Greenberg, D. A., and FitzGerald, O. (2012) HLA associations reveal genetic heterogeneity in psoriatic arthritis and in the psoriasis phenotype. Arthritis Rheum 64, 1134-1144

56. Johnston, A., Gudjonsson, J. E., Sigmundsdottir, H., Love, T. J., and Valdimarsson, H. (2004) Peripheral blood T cell responses to keratin peptides that share sequences with streptococcal M proteins are largely restricted to skin-homing CD8(+) T cells. Clin Exp Immunol 138, 83-93

57. Kim, S. M., Bhonsle, L., Besgen, P., Nickel, J., Backes, A., Held, K., Vollmer, S., Dornmair, K., and Prinz, J. C. (2012) Analysis of the paired TCR alpha- and betachains of single human T cells. PLoS One 7, e37338

58. Chang, J. C., Smith, L. R., Froning, K. J., Kurland, H. H., Schwabe, B. J., Blumeyer, K. K., Karasek, M. A., Wilkinson, D. I., Farber, E. M., Carlo, D. J., and Brostoff, S. W. (1997) Persistence of T-cell clones in psoriatic lesions. Arch Dermatol 133, 703-708

59. Chang, J. C., Smith, L. R., Froning, K. J., Schwabe, B. J., Laxer, J. A., Caralli, L. L., Kurland, H. H., Karasek, M. A., Wilkinson, D. I., Carlo, D. J., and et al. (1994) CD8+ T cells in psoriatic lesions preferentially use T-cell receptor V beta 3 and/or V beta 13.1 genes. Proc Natl Acad Sci U S A 91, 9282-9286

60. The UniProt, C. (2017) UniProt: the universal protein knowledgebase. Nucleic Acids Res 45, D158-D169

61. Kabsch, W. (2010) Xds. Acta Crystallogr D Biol Crystallogr 66, 125-132

62. Evans, P. R., and Murshudov, G. N. (2013) How good are my data and what is theresolution? Acta Crystallogr D Biol Crystallogr 69, 1204-1214

63. McCoy, A. J., Grosse-Kunstleve, R. W., Adams, P. D., Winn, M. D., Storoni, L. C.,and Read, R. J. (2007) Phaser crystallographic software. J Appl Crystallogr 40, 658-674

64. Murshudov, G. N., Skubak, P., Lebedev, A. A., Pannu, N. S., Steiner, R. A., Nicholls, R. A., Winn, M. D., Long, F., and Vagin, A. A. (2011) REFMAC5 for the refinement of macromolecular crystal structures. Acta Crystallogr D Biol Crystallogr 67, 355-367

65. Emsley, P., Lohkamp, B., Scott, W. G., and Cowtan, K. (2010) Features and development of Coot. Acta Crystallogr D Biol Crystallogr 66, 486-501

66. Perrakis, A., Harkiolaki, M., Wilson, K. S., and Lamzin, V. S. (2001) ARP/wARP and molecular replacement. Acta Crystallogr D Biol Crystallogr 57, 1445-1450

67. Smart, O. S., Womack, T. O., Flensburg, C., Keller, P., Paciorek, W., Sharff, A., Vonrhein, C., and Bricogne, G. (2012) Exploiting structure similarity in refinement: automated NCS and target-structure restraints in BUSTER. Acta Crystallogr D Biol Crystallogr 68, 368-380

68. Adams, P. D., Afonine, P. V., Bunkoczi, G., Chen, V. B., Davis, I. W., Echols, N., Headd, J. J., Hung, L. W., Kapral, G. J., Grosse-Kunstleve, R. W., McCoy, A. J., Moriarty, N. W., Oeffner, R., Read, R. J., Richardson, D. C., Richardson, J. S., Terwilliger, T. C., and Zwart, P. H. (2010) PHENIX: a comprehensive Python-based system for macromolecular structure solution. Acta Crystallogr D Biol Crystallogr 66, 213-221

Table 1 - X-ray diffraction data collection and refinement statistics

	Cw6 - ARTE	Cw6 - ARFN	Cw6 - ADAMTSL5
PDB accession code	5W6A	5W69	5W67
Data Collection			
Space Group	$P12_11$	$P2_12_12_1$	$P2_12_12_1$
Wavelength (Å)	0.953700	0.953700	0.953700
Number of images	420	220	1100
Oscillation range per image (°)	1	1	0.1
Detector	ADSC mx2	ADSC mx2	Eiger mx2
Cell dimensions			
a, b, c (Å)	46.2, 137, 71	51.2, 182.4, 223.0	44.1, 81.6, 116.1
a, b, g (°)	90, 107.1, 90	90, 90, 90	90, 90, 90
Resolution range (Å)	48.2 - 1.74 (1.77 - 1.74)	74.34 - 2.80 (2.89 - 2.80)	41.2 - 2.30 (2.38 - 2.30)
R_{pim}	0.03 (0.32)	0.11 (0.51)	0.09 (0.42)
Mn(I) half-set correlation CC(1/2)	0.99 (0.75)	0.99 (0.81)	0.99 (0.69)
I/sI	18.8 (2.7)	11.8 (2.5)	7.5 (3.2)
Total observations	752689 (34359)	473875 (41362)	76137 (6072)
Unique reflections	86176 (4252)	52631 (4512)	19189 (1863)
Completeness (%)	99.6 (92.8)	100 (100)	99.7 (99.9)
Multiplicity	8.7 (8.1)	9.0 (9.2)	4.0 (3.3)
Matthews Coefficient, V_M ($Å^3 Da^{-1}$)	2.66	2.37	2.32
Solvent (%)	53.8	48.03	47.1
Refinement			
Resolution range (Å)	68.5 - 1.74 (1.78 - 1.74)	41.99 - 2.80 (2.87 - 2.80)	41.197 - 2.300 (2.382 - 2.300)
Rwork	0.1605	0.1641	0.1883
Rfree	0.2007	0.2231	0.2347
Biological complexes in ASU	2	4	1
Protein molecules in ASU	6	12	3
Number of atoms			
Protein	6248	12458	3080
Ligands	0	0	24
Water	780	795	223
Average B factor (Å)			
Protein	26.9	35.2	28.8
Ligands	0	0	48.6
Water	33.6	29.4	36.2
RMSD			
Bond lengths (Å)	0.0266	0.010	0.002
Bond Angles (°)	2.3127	1.11	0.505
Ramachandran plot			
Ramachandran allowed (%)	100	100	100
Ramachandran outlier (%)	0	0	0

Table 2 - Putative HLA-C*06:02 restricted psoriasis peptide antigens - A list of putative HLAC*06:02 restricted peptide antigens obtained from literature. Table contains peptide sequences and residues at HLA-C*06:02 anchor positions. A bind score ranging from one (*) to six (*) depending on each anchor residue. Six (*) denotes a peptide that has all favoured residues in the anchor residues and a (-) denotes all unfavourable residues.

Name	Protein	Sequence	P2	P7	P9	Bind Score	Reference
LL37p6s	LL37	RIKDFLRNL	I	R	L	*	[13]
LL37p7s	LL37	FLRNLVPRT	L	P	T	-	[13]
LL37p4s	LL37	EFKRIVQRI	F	Q	I	**	[13]
LL37p4sb	LL37	KEFKRIVQR	E	V	R	*	[13]
LL37p5s	LL37	RIVQRIKDF	I	R	F		[13]
$ADAM_{57-65}$	ADAMTSL5	VRSRRCLRL	R	L	L	*	[14]
125K17-9	Keratin17	RLASYLDKV	L	D	V	*	[31]
128K17-9	Keratin17	SYLDKVRA	Y	V	A	**	[31]
134K17-12	Keratin17	RALEEANADLEV	A	L	V	**	[31]
135K17-9	Keratin17	ALEEANADL	L	A	L	**	[31]
139K17-9	Keratin17	ANADLEVKI	N	V	I	**	[31]
217K17-9	Keratin17	DVNGLRRVL	V	R	L	*	[31]
220K17-9	Keratin17	GLRRVLDEL	L	D	L	**	[31]
231K17-9	Keratin17	ARTDLEMQI	R	M	I		[31]
238-K17-9	Keratin17	QIEGLKEEL	I	E	L	**	[31]
261M6-9	Strep M6	DIGALKQEL	I	Q	L		[31]
282M6-9	Strep M6	SRKGLRRDL	R	R	L		[31]
324M6-9	Strep M6	SRQGLRRDL	R	R	L		[31]
327M6-9	Strep M6	GLRRDLDAS	L	D	S	-	[31]
384M6-9	Strep M6	EAKALKEQL	A	E	L		[31]
338M6-12	Strep M6	AKKQVEKALEEA	K	E	A	-	[31]
344M6-12	Strep M6	KALEEANSKLAA	A	L	A	*	[31]
345M6-9	Strep M6	ALEEANSKL	L	S	L	**	[31]
354M6-12	Strep M6	AALEKLNKELEE	A	L	E	*	[31]
355M6-9	Strep M6	ALEKLNKEL	L	K	L		[31]
127K17-9	Keratin17	ASYLDKVRA	S	V	A	**	[31]
130K17-9	Keratin17	LDKVRALEE	D	L	E	-	[31]
31K17-12	Keratin17	ISSVLAGASCPA	S	C	A	*	[31]
464M6-12	Strep M6	ALTVMATAGVAA	L	V	A	*	[31]

Figure legends

Figure 1 - Analysis of peptides eluted from HLA-C*06:02.
(A) Length distribution of HLA-C*06:02 presented peptides. (B) Peptide preference motif obtained for peptide nonamers for membrane bound HLA-C*06:02. Dominant, Strong and Preferred amino acids occur at frequencies of >30%, >20% and >10% respectively. (C) Sequence Logo of nonomer peptides of membrane bound HLA-C*06:02. Enriched amino acids are shown above and depleted are shown below. Height of amino acids are proportional to frequency of occurrence. Sequence Logos were generated with Seq2Logo server as a p-weighted Kullback-Leibler logo. (D) Overlap of peptide nonamers from membrane bound and soluble HLA-C*06:02. (E) Peptide preference motif obtained for peptide nonamers from soluble HLA-C*06:02. (F) Sequence Logo of nonomer peptides of soluble HLA-C*06:02.

Figure 2 - Overall structures of the peptide-binding grooves of HLA-C*06:02-ARTE, ARFN and ADAMTSL5.
The a2 helix has been removed for clarity. In grey is the simulated annealing F_O-F_C omit electron density surrounding the peptide ligands, contoured at 3 s. (A) The HLA-C*06:02 peptide-binding groove represented as cartoon (teal) with the ARTE peptide as sticks (yellow). (B-C) The ARFN peptide was observed in two conformations in the asymmetric unit. (B) The ARFN-1 confirmation with the HLA represented as cartoon (blue) and the peptide as sticks (green). (C) The ARFN-2 conformation with the HLA represented as cartoon (lime green) and the peptide as sticks (blue). (D) The ADAMTSL5 peptide. The HLA is represented as cartoon (green) and the peptide as sticks (wheat). (E) Overlay of Ca traces of HLA-C*06:02 structures. The regions of difference at the b1-b2 loop and a2 helical hinge are labelled. (F) Overlay of the HLA-C*06:02 peptide ligands.

Figure 3 - Structure of HLA-C*06:02-ARTE. (A) The ARTE peptide within HLA-C*06:02 peptide binding groove.
Residues 1 - 126 of the HLA are represented as cartoon (teal) and the ARTE peptide is shown as yellow sticks. The pockets of the peptide binding groove are represented as grey discs and labelled A-F. (B) The B pocket of HLA-C*06:02. Contacts between the P2 arginine anchor (yellow sticks) and side chains of HLA-C*06:02 residues (orange sticks). (C) The E pocket of HLA- C*06:02. Contacts between the P7 arginine anchor (yellow sticks) and side chains of HLA-C*06:02 residues (orange sticks). (D) The F pocket of HLA-C*06:02. Contacts between the P leucine anchor (yellow sticks) and side chains of HLA-C*06:02 (orange sticks).

Figure 4 - Comparison of the two conformations of ARFN peptide observed in the crystal structure.
First conformation of ARFN (ARFN-1) represented as sticks (green) with the HLA represented as cartoon (grey) with HLA sidechains contacting the peptide shown as sticks (pink). The second conformation of the ARFN (ARFN-2) peptide is represented as sticks (blue) the HLA represented as cartoon (grey) with HLA sidechains contacting the peptide shown as sticks (pink). (A) Conservation of contacts between the HLA and the ARFN-1 and ARFN-2 peptides at the P2-Arg position. (B) Conservation of contacts between the HLA and the ARFN-1 and ARFN-2 peptides at the P -Val position. (C) The ARFN-1 and ARFN-2 conformations differ in the orientation of their P7-Arg side chain. The P7-Arg of ARFN-1 forms a salt-bridge with Asp9 whereas the P7-Arg of ARFN-2 is shifted 5.8 Å and forms a salt-bridge with Asp114. (D) Plasticity of Trp97 was observed between the HLA-C*06:02-ARTE and ARFN structures. The ARTE, ARFN-1 and ARFN-2 peptides are shown as yellow, green and blue sticks respectively. The Trp97 observed in the ARTE complex (orange sticks) is rotated 140° compared to the Trp97 of the ARFN complex (pink sticks).

Figure 5 - Structure of HLA-C*06:02-ADAM peptide analogue (VRSRR-abu-LRL).
(A) View of ADAMTSL5 peptide analogue (VRSRR-abu-LRL) within the HLA-C*06:02 peptide binding groove, with the □2 helix removed for clarity. The HLA-C*06:02 residues 1 - 126 are represente cartoon (green) with sidechains within 3.4 Å represented as sticks (blue). The ADAMTSL5 peptide is represented sticks (wheat). (B) Overlay of P7-Arg of HLA-C*06:02-ARTE, represented as sticks (grey), with the P7-Leu of ADAMTSL5 represented as sticks (wheat). Plasticity of Trp97 was observed between the HLA-C*06:02-ARTE and the ADAMTSL5 structure. The ARTE peptide is coloured grey, the ADAMSTL5 peptide is coloured wheat. The Trp97 observed in the ARTE complex (orange sticks) is rotated 114° compared to the Trp97 of the ADAMSTL5 complex (blue sticks).

Figure 6 - Comparison of available HLA-C structures.
(A) Ca trace overlay of HLA-C*06:02 (teal), HLA-C*03:04 (PDB: 1EFX) (green), HLA-C*04:01 (PDB: 1QQD) (pink), HLA-C*05:01 (PDB: 5VGD) (purple), HLA-C*07:02 (PDB: 5VGE) (yellow), HLA-C*08:01 (PDB: 4NT6) (wheat) and HLA-B*27:05 (PDB: 3BP4) (blue). Surface electrostatics of (B) HLA-C*06:02 ARTE (C) HLA-C*04:01, (D) HLA-C*03:04 (E) HLA-C*05:01, (F) HLA-C*08:01 (G) HLA-C*07:02 and (H) HLA-B*27:05. B and E-pockets are shown as yellow circles. Generated using APBS Tools plugin within PyMOL.

Figure 7 - A comparison of the anchor pockets of HLA-C*06:02 with other HLA-C alleles.
(A) Sequence alignment of the B-, E- and F-pockets of common HLA-C molecules. Residues conserved with HLA- C*06:02 are shown as a dash (-). (B - G) A structural comparison of the anchor pockets of HLA-C*06:02 and HLA-C*04:01 (PDB: 1QQD). The HLA-C*06:02-ARTE peptide is represented as yellow sticks. The alternate conformation of the P7- Arg of the ARFN peptide is shown as blue sticks. The HLA-C*06:02 pocket residues are shown as teal sticks and van de Waals surface (VDW). The HLA-C*04:01 peptide represented as pink sticks. The HLA-C*04:01 pocket residues are shown as purple sticks and VDW surface. Panels (B and C) The B pocket. Panels (D and E) The E pocket. Panels (F and G) The F pocket.

Figure 1

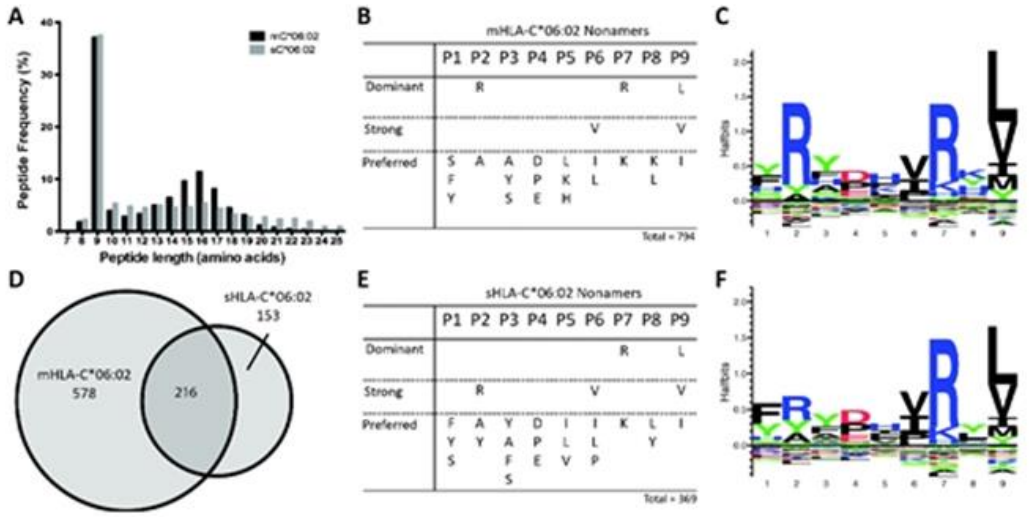
A
mC*06:02
sC*06:02
Peptide Frequency (%)
Peptide length (amino acids)
B
mHLA-C*06:02 Nonamers
P1 P2 P3 P4 P5 P6 P7 P8 P9
Dominant R R L
Strong V V
Preferred S A A D L I K K I
F Y P K L L
Y S E H
Total = 794
C
Halfbits
D
sHLA-C*06:02
153
mHLA-C*06:02
578
216
E
sHLA-C*06:02 Nonamers
P1 P2 P3 P4 P5 P6 P7 P8 P9
Dominant R L
Strong R V V
Preferred F A Y D I I K L I
Y Y A P L L Y
S F E V P
S
Total = 369
F
Halfbits

Figure 2

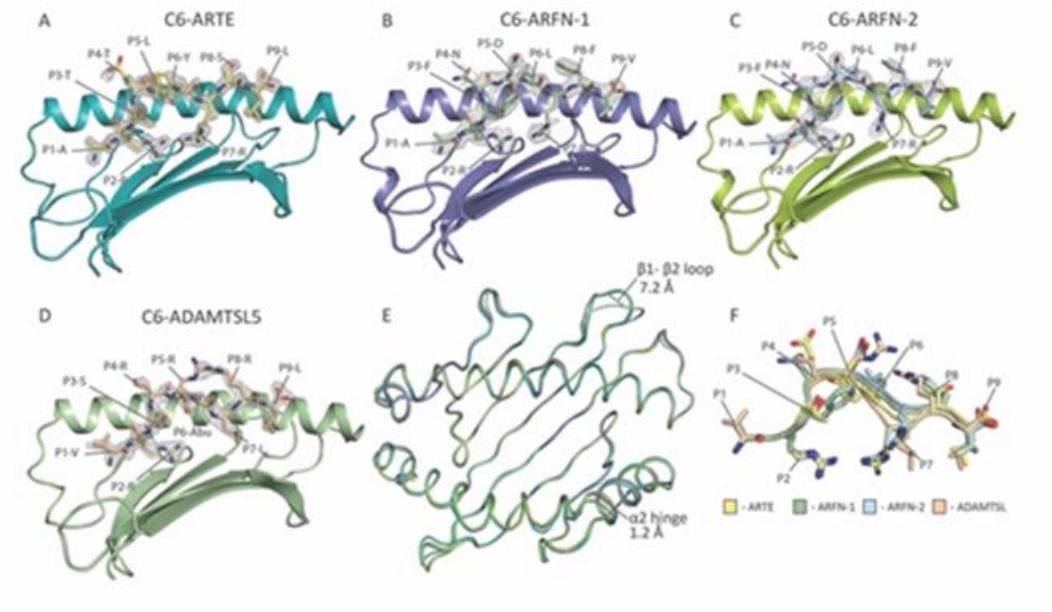
A
C6-ARTE
B
C6-ARFN-1
C
C6-ARFN-2
D
C6-ADAMTSL5
E
β1- β2 loop
7.2 Å
α2 hinge
1.2 Å
F
ARTE
ARFN-1
ARFN-2
ADAMTSL

Figure 3

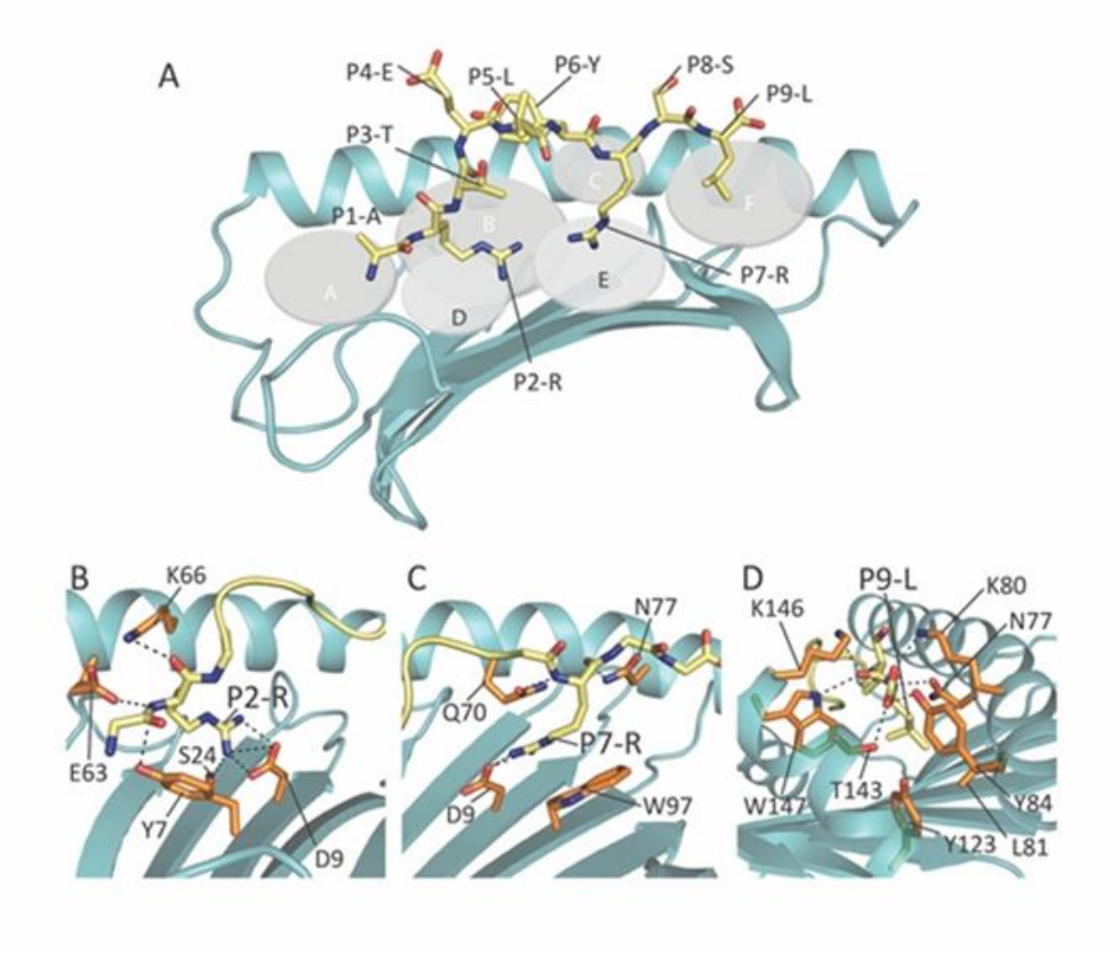
A
P4-E
P5-L
P6-Y
P8-S
P9-L
P3-T
P1-A
P7-R
P2-R
A
B
C
D
E
F
B
K66
P2-R
E63
S24
Y7
D9
C
N77
Q70
P7-R
D9
W97
D
P9-L
K80
K146
N77
W147
T143
Y84
Y123
L81

Figure 4

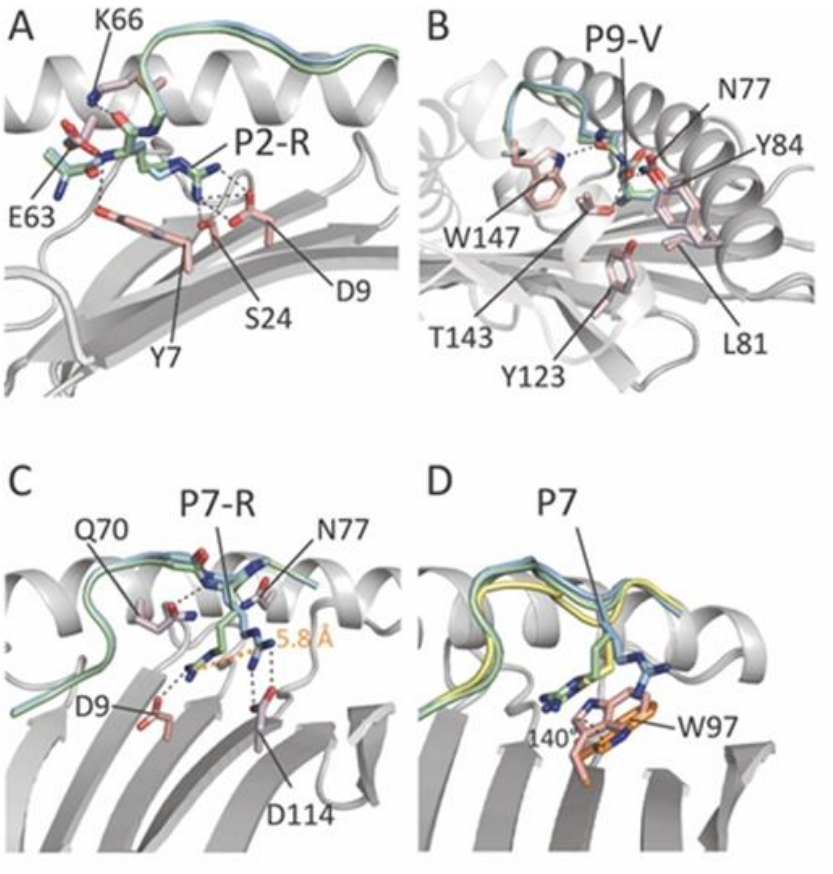
A
K66
P2-R
E63
D9
S24
Y7
B
P9-V
N77
Y84
W147
T143
L81
Y123
C
P7-R
Q70
N77
5.8 Å
D9
D114
D
P7
W97
140°

Figure 5

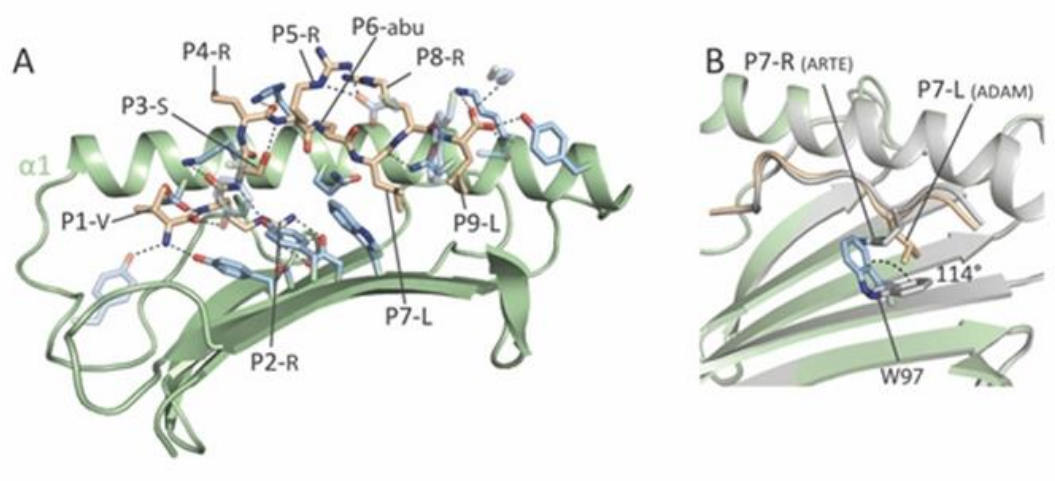
A
P5-R
P6-abu
P4-R
P8-R
P3-S
α1
P1-V
P9-L
P7-L
P2-R
B
P7-R (ARTE)
P7-L (ADAM)
114°
W97

Figure 6

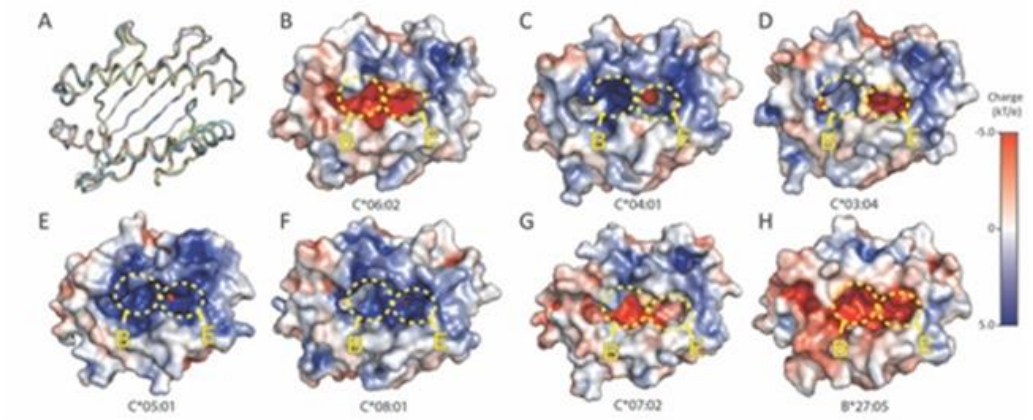
A
B
C
D
C*06:02
C*04:01
C*03:04
Charge (kT/e)
-5.0
0
5.0
E
F
G
H
C*05:01
C*08:01
C*07:02
B*27:05

Figure 7

Pocket	B Pocket											E Pocket						F Pocket										
Residue	9	22	24	34	45	67	7	63	66	70	99	97	114	116	147	152	156	77	95	81	116	80	84	123	124	143	146	147
C*06:02	D	F	S	V	G	Y	Y	E	K	Q	Y	W	D	S	W	E	W	N	L	L	S	K	Y	Y	I	T	K	W
C*01:02	F	-	-	-	-	-	-	-	-	-	C	-	-	Y	-	-	R	S	-	-	Y	N	-	-	-	-	-	-
C*02:02	Y	-	A	-	-	-	-	-	-	-	-	R	-	-	-	-	-	-	-	-	-	-	-	-	-	-	-	-
C*03:02	Y	-	A	-	-	-	-	-	-	-	-	R	-	-	-	-	L	S	-	-	-	N	-	-	-	-	-	-
C*03:03	Y	-	A	-	-	-	-	-	-	-	-	R	-	Y	-	-	L	S	I	-	Y	N	-	-	-	-	-	-
C*03:04	Y	-	A	-	-	-	-	-	-	-	-	R	-	Y	-	-	L	S	I	-	Y	N	-	-	-	-	-	-
C*04:01	S	-	A	-	-	-	-	-	-	-	F	R	N	F	-	-	R	-	-	-	F	-	-	-	-	-	-	-
C*04:03	Y	-	A	-	-	-	-	-	-	-	F	R	N	F	-	-	R	-	-	-	F	-	-	-	-	-	-	-
C*05:01	Y	-	A	-	-	-	-	-	-	-	-	R	N	F	-	-	R	-	-	-	F	-	-	-	-	-	-	-
C*06:03	Y	-	-	-	-	-	-	-	-	-	-	-	-	-	-	-	-	-	-	-	-	-	-	-	-	-	-	-
C*06:04	-	-	-	-	-	-	-	-	-	-	-	-	-	-	-	-	L	-	-	-	-	-	-	-	-	-	-	-
C*06:06	-	-	-	-	-	-	-	-	-	-	-	-	-	-	-	-	R	-	-	-	-	-	-	-	-	-	-	-
C*06:08	-	-	-	-	-	-	-	-	-	-	-	-	-	-	-	-	-	-	-	-	-	-	-	-	-	-	-	-
C*06:09	-	-	-	-	-	-	-	-	-	-	-	-	N	F	-	-	-	-	-	-	F	-	-	-	-	-	-	-
C*07:01	-	-	-	-	-	-	-	-	N	-	-	R	-	-	L	A	L	S	-	-	-	N	-	-	-	-	-	L
C*07:02	-	-	-	-	-	-	-	-	-	-	S	R	-	-	L	A	L	S	-	-	-	N	-	-	-	-	-	L
C*07:03	-	-	-	-	-	-	-	-	-	-	S	R	-	-	-	A	L	S	-	-	-	N	-	-	-	-	-	-
C*07:04	-	-	-	-	-	-	-	-	-	-	-	R	-	F	L	A	D	S	F	-	F	N	-	-	-	-	-	L
C*08:01	Y	-	A	-	-	-	-	-	-	-	-	R	N	F	-	T	L	S	-	-	F	N	-	-	-	-	-	-
C*08:02	Y	-	A	-	-	-	-	-	-	-	-	R	N	F	-	-	R	S	-	-	F	N	-	-	-	-	-	-
C*08:03	Y	-	A	-	-	-	-	-	-	-	-	R	N	F	-	T	L	S	-	-	F	N	-	-	-	-	-	-
C*12:03	Y	-	A	-	-	-	-	-	-	-	-	-	-	-	-	-	-	S	-	-	-	N	-	-	-	-	-	-
C*14:02	S	-	A	-	-	-	-	-	-	-	F	-	-	-	-	-	R	S	-	-	-	N	-	-	-	-	-	-
C*15:02	Y	-	A	-	-	-	-	-	N	-	-	R	-	L	-	-	L	-	I	-	L	-	-	-	-	-	-	-
C*16:01	Y	-	A	-	-	-	-	-	-	-	-	-	-	-	-	A	Q	S	-	-	-	N	-	-	-	-	-	-
C*17:01	Y	-	A	-	-	-	-	-	-	-	-	R	N	F	L	-	L	-	I	-	F	-	-	-	-	A	-	L